THE JOURNAL OF BIOLOGICAL CHEMISTRY VOL. 288, NO. 10, pp. 7351–7362, March 8, 2013

Transient Influx of Nickel in Root Mitochondria Modulates Organic Acid and Reactive Oxygen Species Production in Nickel Hyperaccumulator *Alyssum murale*[*] [S]

Received for publication, August 1, 2012, and in revised form, December 20, 2012 Published, JBC Papers in Press, January 15, 2013, DOI 10.1074/jbc.M112.406645

Bhavana Agrawal[‡§], **Kirk J. Czymmek**[§¶], **Donald L. Sparks**[‡§‖], **and Harsh P. Bais**[‡§‖1]

From the Departments of [‡]*Plant and Soil Sciences and* [¶]*Biological Sciences, University of Delaware, Newark, Delaware 19716, the* [§]*Delaware Biotechnology Institute, Newark, Delaware 19711, and the* [‖]*Center for Critical Zone Research, Newark, Delaware 19711*

Background: Mitochondria are important targets of metal toxicity.
Results: Our data confirms that nickel is localized in the mitochondria of *Alyssum murale* root epidermal cells.
Conclusion: The interaction of nickel with mitochondria is imperative in nickel uptake.
Significance: The results obtained from our studies will help to understand the role of biochemical processes in nickel uptake.

Mitochondria are important targets of metal toxicity and are also vital for maintaining metal homeostasis. Here, we examined the potential role of mitochondria in homeostasis of nickel in the roots of nickel hyperaccumulator plant *Alyssum murale*. We evaluated the biochemical basis of nickel tolerance by comparing the role of mitochondria in closely related nickel hyperaccumulator *A. murale* and non-accumulator *Alyssum montanum*. Evidence is presented for the rapid and transient influx of nickel in root mitochondria of nickel hyperaccumulator *A. murale*. In an early response to nickel treatment, substantial nickel influx was observed in mitochondria prior to sequestration in vacuoles in the roots of hyperaccumulator *A. murale* compared with non-accumulator *A. montanum*. In addition, the mitochondrial Krebs cycle was modulated to increase synthesis of malic acid and citric acid involvement in nickel hyperaccumulation. Furthermore, malic acid, which is reported to form a complex with nickel in hyperaccumulators, was also found to reduce the reactive oxygen species generation induced by nickel. We propose that the interaction of nickel with mitochondria is imperative in the early steps of nickel uptake in nickel hyperaccumulator plants. Initial uptake of nickel in roots results in biochemical responses in the root mitochondria indicating its vital role in homeostasis of nickel ions in hyperaccumulation.

Despite the rapid developments being made in the field of metallomics, the interactions and functions of metal ions in various cellular organelles remain obscure. The expeditions of the metal ions from the environment to a particular cellular organelle are intricately complicated because of influences from several biological and environmental processes. It is particularly challenging to trace metal ions in their complicated geochemical forms in the environment, to their mobilization and transformation in biochemical forms in diverse tissues, cells, and organelles. Once within the tissues, metals ions typically associate with intra- and extracellular ligands, which are usually specific to a particular metal species. Furthermore, the investigation of the role of metal ions in cellular organelles can be difficult because of the complex and transient interactions that these metal ions can undergo with cellular metabolites on its way to different cellular organelles. Finally, the intra-organelle metal ions either interact with molecules in the membranes or find their way into specific cellular organelles to evoke vital cellular responses that are chiefly specific to particular metal ion chemical properties.

Essential metals are required for optimum plant growth but when present in excess in the environment and soil, they are absorbed by roots and translocated to different parts of the plant, leading to impaired metabolism and reduced growth. A rare group of extremophiles in the plant kingdom commonly called metal hyperaccumulators have attracted considerable interest in past two decades because of their commercial importance in phytoremediation technologies (1, 2). Of these metal hyperaccumulators, nickel hyperaccumulators have been studied the most, possibly due to their availability in large numbers. Approximately, 400 species of nickel hyperaccumulators have been documented, mostly belonging to the family *Cruciferae* (3). Nickel hyperaccumulator plants are not only tolerant of high concentrations of nickel but are also particularly proficient in its uptake via roots, transport through xylem, and storage in leaves in detoxified form. *Alyssum murale*, a member of the *Cruciferae* family, is considered highly desirable for phytoremediation and has been well studied. However, the molecular and cellular basis of nickel hyperaccumulation remains elusive.

Detoxification of nickel ions in hyperaccumulator plants is achieved by their sequestration to vacuoles (4–8) and subsequent chelation to ligands present therein (8–12). Cellular or tissue compartmentalization and sequestration of nickel has been studied widely (4, 6, 7, 13–18), however, few studies focus on organelle distribution of nickel (4, 7, 8). These studies converge on vacuolar distribution of nickel, whereas its effect on other cellular organelles was not defined. Our lack of knowledge on the effect of nickel on cellular organelles in hyperaccumulators limits understanding of the sequestration of nickel ions to vacuoles. This is particularly important because cellular

* This work was supported by National Science Foundation Grant EPSCoR (to H. P. B., K. J. C., and D. L. S.).
[S] This article contains supplemental Figs. S1–S3.
[1] To whom correspondence should be addressed. E-mail: hbais@udel.edu.

organelles, specifically chloroplast and mitochondria, respond to excess nickel by producing ROS, which induces apoptosis of the cells (20–22).

Mitochondria play a pivotal role in cellular metal ion homeostasis and are also an important target of heavy metal toxicity. Among the myriad of functions mitochondria perform for the cell, the most important one indisputably is the production of adenosine 5′-triphosphate (ATP) utilizing the Krebs cycle (23). When ATP is synthesized, organic acids are produced as side products in mitochondria and their metabolic levels are constantly regulated. Mitochondria are also important intracellular sites for production of ROS. The regulation of reactive oxygen species (ROS)[2] production is important for cell growth (24), gravitropic responses (25), and other normal cell operations. The ROS produced by mitochondria under normal physiological conditions are a side product of electron transport redox reactions in the respiratory chain. However, ROS are also produced in biotic as well as abiotic stress, such as in response to metals. Nickel uptake in plants results in increased ROS (20, 26–28). Changes in the redox potential of mitochondrial membrane, which are attributable to enhanced ROS production and depletion of reduced glutathione (GSH), facilitate opening of mitochondrial permeability transition pore and induction of apoptosis.

The roots of hyperaccumulator plants are the first line of contact to high concentrations of heavy metal ions in soil. This prompted us to investigate the role of mitochondria in metal homeostasis in the roots of the hyperaccumulator plant *A. murale*. To achieve this objective we utilized a study model based on comparative analysis of nickel-induced responses in *A. murale* (hyperaccumulator) and *A. montanum* (non-accumulator). Here, we show that the initial steps of nickel exposure result in rapid and transient nickel influx in the root mitochondria of hyperaccumulator *A. murale* and not in non-accumulator *A. montanum*. In roots, the mitochondrial Krebs cycle functions are modulated in response to nickel in favor of production of organic acids such as malic and citric acid. Interestingly, we also found that malic acid is instrumental in reducing excess ROS generation in post-nickel treatment of roots. Our results suggest that the mitochondria of hyperaccumulator plants may have adapted in circumventing the toxic effects of nickel-triggered ROS and therefore may have an important role in the metal hyperaccumulation process. The methods and findings discussed will help in understanding the role of novel metabolic and biochemical processes that are involved in enhancing plant fitness against heavy metal toxicity.

EXPERIMENTAL PROCEDURES

Plant Material, Reagents, and Control—All chemicals used in the study were of reagent grade. Newport Green™ DCF diacetate, 2,7-dichlorodihydrofluorescein diacetate (H_2DCFDA) and MitoTracker® Red CMXRos were purchased from Molecular Probes (Eugene, OR). All other chemical and enzymes were purchased from Sigma or Fisher Scientific Company. Nickel (II) nitrate ($Ni(NO_3)_2$) was purchased from Sigma. The anhydrous form is not commonly found, thus "Ni(II) nitrate" usually refers to nickel (II) nitrate hexa-hydrate ($Ni(NO_3)_2{\cdot}6H_2O$). It is important to note that nickel compounds are carcinogenic and should be handled with proper care. Seeds of *A. murale* were provided by Dr. Rufus Chaney (United States Department of Agriculture, Beltsville, MD). To employ as a comparative control, seeds of *A. montanum* were purchased from Park Seed® Wholesale Inc., Greenwood, SC.

Establishment of Axenic in Vitro Plant Culture for A. murale and Alyssum montanum—Seeds of nickel hyper- and non-accumulator (*A. murale* and *A. montanum,* respectively) were surface sterilized with 2.5% (v/v) sodium hypochlorite (NaOCl). The seeds were rinsed with several flushes of sterile water and placed on sterilized 3% Murashige and Skoog (MS) agar plates for germination. Post-germination seedlings were transferred to 3% MS liquid medium (pH 5.8) supplemented with 5 μM Fe-HBED. Seedlings were allowed to grow in multiwell plates or in magenta boxes with a mesh to sustain growth of roots and aerial parts separately. Seedlings were grown for 10–15 days. For the treatments of plants, media was spiked with nickel at concentrations appropriate to the experiment in the form of $Ni(NO_3)_2$ under sterile conditions. Fresh samples of roots were harvested and analyzed for physiological determinations. Parts of the plant material were frozen in liquid nitrogen and kept at −80 °C for further molecular analyses.

Plant Weight and Root Length as the Measure of Nickel Tolerance—To compare nickel tolerance of the two species, seeds were germinated on 1.5% MS agar medium (pH 5.7–5.8). Post-germination seedlings were transferred to 1.5% MS liquid medium (pH 5.7–5.8) supplemented with 5 μM Fe-HBED. Two replicates (12 seedlings per treatment) for each of the two species were treated with $Ni(NO_3)_2$ or were not treated for their use as controls. Eight days post-transfer the seedlings were harvested and their root lengths and plant weights were measured to estimate nickel tolerance. Observations on total plant biomass treated and untreated with nickel were recorded and percent inhibition in growth post-nickel treatment was calculated.

Isolation and Purification of Root Mitochondria—Mitochondria were isolated from the roots of the treated *A. murale* and *A. montanum* plants as described by (29). Tissues were homogenized in extraction buffer (90 mM sodium pyrophosphate, 900 mM sucrose, 6 mM EDTA, 0.9% (w/v) BSA, 2.4% (w/v) polyvinylpyrrolidone 25, 9 mM cysteine, 15 mM glycine, 6 mM β-mercaptoethanol, pH 7.5). Following filtration through a nylon net (100 μm mesh), crude mitochondria were recovered by two cycles of low speed (1,500 × *g*) and high speed (16,000 × *g*) centrifugation with intermediate re-suspension in washing buffer (10 mM potassium phosphate, 300 mM sucrose, 1 mM EDTA, 0.1% (w/v) BSA, 5 mM glycine, pH 7.5). The re-suspended second pellet was loaded on a 30% (v/v) Percoll solution in washing buffer and centrifuged for 1 h at 40,000 × *g*. Mitochondria were recovered in the bottom third of the Percoll gradient established during centrifugation and washed twice.

Protein Estimation—Frozen mitochondria were completely lysed by two freeze/thaw cycles (liquid nitrogen, 30 °C water bath). Protein content was determined with a Bio-Rad 500–

[2] The abbreviations used are: ROS, reactive oxygen species; H_2DCFDA, 2,7-dichlorodihydrofluorescein diacetate; MS, Murashige and Skoog; Fe-HBED, *N*,*N*′-di-(2-hydroxybenzoyl)-ethylenediamine-*N*,*N*′-diacetic acid; ICP-AES, inductively coupled plasma-atomic emission spectroscopy.

006 kit (Bio-Rad) based on the Bradford dye binding procedure that utilizes the color change of Coomassie Brilliant Blue G-250 (30), Sigma BSA (A-2153) was used as standard.

Estimation of Enzymatic Activities in the Purified Mitochondrial Fractions—Enzymatic assays were conducted on either intact mitochondrial fractions or mitochondrial extracts following isolation of mitochondria from the plant roots subjected to nickel treatment at different time intervals. The integrity of the outer mitochondrial membrane was assessed by measuring cytochrome *c* oxidase (COX, EC 1.9.3.1) activity spectrophotometrically at 25 °C by following the absorbance increase at $\lambda_{550\ nm}$ in the presence and absence of the detergent, *n*-dodecyl β-D-maltoside (31, 32). The percentage of mitochondrial integrity was calculated as: $100 \times ((\Delta A/min_{with\ detergent}) - (\Delta A/min_{without\ detergent}))/(\Delta A/min_{with\ detergent})$. For citrate synthase (CS, EC 1.11.1.6), which is an enzyme of the mitochondrial matrix, the activity was assayed by adding 100 μM 5,5′-dithiobis(nitrobenzoic acid), 300 μM acetyl-CoA, 500 μM oxaloacetate, 100 mM Tris-HCl (pH 8.1) in a total reaction volume of 200 μl. Measurements were carried out spectrophotometrically at 25 °C by monitoring the reduction of acetyl-CoA to CoA, at $\lambda_{412\ nm}$ (33, 34). Malate dehydrogenase (L-malate:NAD^+ oxidoreductase, EC 1.1.1.37) was assayed in the direction of malate oxidation (forward reaction) spectrophotometrically at $\lambda_{340\ nm}$ in 200 μl of buffer containing 0.25 M glycine, 0.20 M hydrazine, 2.7 mM NAD^+ adjusted to pH 9 (35). Malate dehydrogenase activity was assayed in the direction of NADH oxidation (backward reaction) according to Ref. 36. The decrease in absorbance at $\lambda_{340\ nm}$ was determined in a 200-μl reaction mixture (pH 7.2) containing the following: 94.6 mM phosphate buffer (pH 6.7), 0.2 mM NADH sodium salt, 0.5 mM oxalacetic acid, and 1.67 mM $MgCl_2$, at 25 °C.

Imaging for Intracellular nickel—To investigate the intracellular distribution of ionic nickel in the roots, the green fluorescent Newport Green™ DCF diacetate indicator dye was used. The seedlings of *A. murale* and *A. montanum* were treated with $Ni(NO_3)_2$ at 200 and 700 μM for 20 min and 1 h or were left untreated (control). Nickel staining dye Newport Green DCF diacetate was added to a final concentration of 30 μM. Newport Green DCF has been demonstrated to be able to penetrate the cell membrane and is a very sensitive indicator of nickel ions. Although Newport Green DCF can also detect higher concentrations of zinc and cobalt ions, it is insensitive to other metal ions such as calcium, manganese, iron, copper, lead, and mercury. Root cells were imaged on a Zeiss LSM 510 confocal microscope using a ×40 C-Apochromat water immersion objective (numerical aperture = 1.2). The excitation wavelength for Newport Green DCF diacetate was 488 nm with a 505-nm long pass emission filter.

Dual Fluorescence Labeling for Intracellular Nickel and Mitochondria—The seedlings of *A. murale* and *A. montanum* were treated with $Ni(NO_3)_2$ at 200 and 700 μM and incubated at 30 °C for 1 h. In the next step, nickel staining dye Newport Green DCF diacetate was added to a final concentration of 30 μM and roots were incubated for another 15 min at the same temperature. Finally, MitoTracker Red CMXRos dye was added at 50 nM and samples were immediately visualized under the confocal microscope. Cells were imaged in fast-line switch mode on a Zeiss CLSM 510 confocal microscope using a ×40 C-Apochromat water immersion objective (numerical aperture = 1.2). The excitation wavelength for Newport Green DCF diacetate was 488 nm with a 500–550 nm band pass emission filter, and for MitoTracker Red CMXRos we used a 561-nm laser excitation with a 600-nm long pass emission filter. In dual labeling experiments, we used the fast-line switch mode to ensure no signal bleed-through between channels. Inadequate penetration of nickel ions and/or dye due to short incubation (20 min) resulted in the formation of patches of the dual stained epithelial cells. Also incubation of roots with both the dyes simultaneously for >15 min appeared to be toxic for the root epithelial cells.

Imaging for nickel in Purified Mitochondria—Mitochondrial fractions (5 μl) were stained with 10 μM Newport Green DCF diacetate and 20 nM MitoTracker Red CMXRos for 5 min. Nickel in purified mitochondria were visualized by confocal microscopy as described above.

Imaging for ROS in the Roots—ROS imaging was performed by slightly modifying the previously reported protocol (24). One-week-old *A. murale or A. montanum* seedlings germinated on MS solid medium with 3% sucrose were transferred to MS liquid medium with 1.5% sucrose and pre-treated with 50 μM malic acid for 1 h or were left untreated (control). Pre-treated or control roots were treated again with or without 80 μM $Ni(NO_3)_2$. After 10 min, 2.5 μM H_2DCFDA dissolved in dimethyl sulfoxide (less than 0.001% final concentration) procured from Invitrogen were added to the roots and incubated for 30 min at 4 °C. The roots were then washed twice with 0.1 mM KCl, 0.1 mM $CaCl_2$ (pH 6.0). The washed roots were incubated in MS liquid medium with 1% sucrose for another 30 min at room temperature. The roots were imaged by using laser excitation wavelength of 488 nm with a 505-long pass emission filter. The images were acquired at 512 × 512 pixel resolution with a *Z*-stack scan through the whole root. Images were captured with a ×10 C-Apoochromat water immersion objective (numerical aperture 0.45) on a Zeiss LSM 510 confocal microscope. Quantitative analysis was performed by determining the average pixel intensity per unit area using ImageJ (rsb.info.nih.gov/ij/).

Determination of Nickel Content in Plant Sample—Nickel was estimated by slightly modifying the previously reported protocol (8). For nickel estimation, plant samples were thoroughly washed and oven dried at 60 °C for 3 days. Samples were subsequently digested at 120 °C for 60 min in 3 ml of concentrated nitric acid. Samples were cooled to room temperature and 600 μl of 30% (w/v) hydrogen peroxide was added. This mixture was heated at 120 °C for 20 min, cooled, and deionized water was added to a final volume of 6 ml. Nickel concentrations were measured using inductively coupled plasma-atomic emission spectroscopy (ICP-AES). For determination of nickel in mitochondria, purified mitochondrial fractions (1 ml) mixed with an equal volume of concentrated nitric acid were heated at 120 °C. Samples were cooled to room temperature and 400 μl of 30% (w/v) hydrogen peroxide was added. This mixture was heated at 120 °C for 20 min, cooled, and deionized water was added to a final volume of 4.5 ml. Mitochondrial wash extracts were used as negative control. In mitochondria, nickel was ana-

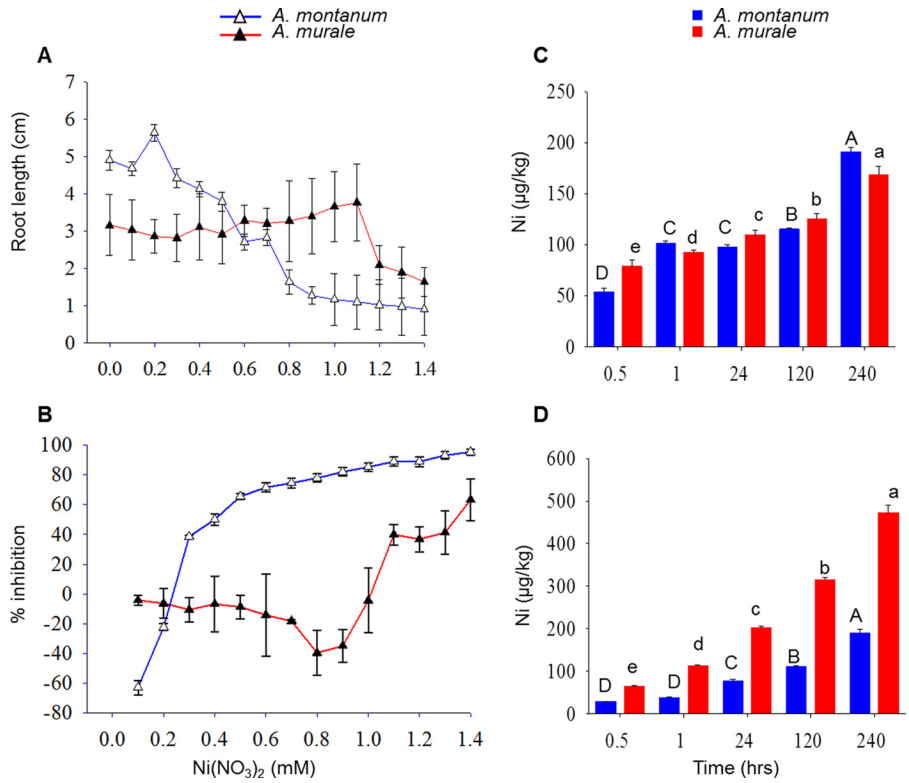

FIGURE 1. **Comparison of tolerance, root absorption, and translocation of nickel in hyperaccumulator *A. murale* and non-accumulator *A. montanum*.** *A,* relative root growth increment in *Alyssum species* in response to various concentrations of nickel in solution culture after 10 days exposure. Values are mean ± S.D. *B*, percentage inhibition in growth in *Alyssum species* in response to various concentrations of nickel in solution culture after 10 days exposure. Values are mean ± S.D. Relative nickel accumulations in the roots (*C*) and shoots (*D*) of *Alyssum species* w.r.t treatment duration. Plants of both the species were treated with 700 μM $Ni(NO_3)_2$ for different time intervals. Roots and shoots of treated and control plants were sampled and nickel was estimated using ICP-AES as described under "Experimental Procedures." Significant differences among the treatments at $p < 0.05$ were determined by one-way analysis of variance followed by Tukey-Kramer test ($\alpha = 0.5$) and are indicated by *different letters*. Values are mean ± S.D.

lyzed by ICP-AES, and normalized by the amount of total mitochondrial proteins in the samples.

Semiquantitative RT-PCR—Total RNA from nickel-treated and untreated *Alyssum* roots was extracted using the TRIzol reagent (Invitrogen) according to the manufacturer's protocol. RNA was also extracted from aluminum-treated and untreated *Alyssum* roots. *Alyssum* roots treated with aluminum chloride (4 μM) for 24 h were also used to isolate RNA for expression analysis. The RNA was treated with DNase I (Promega) at 37 °C for 10 min to remove genomic DNA. RNA was stored at −80 °C until further use. The first strand cDNA was synthesized with 2 μg of purified total RNA using the RT-PCR system (Promega) according to the manufacturer's protocol. The PCR conditions were as follows: 0.5 μl of RT product was amplified in a 25-μl volume containing 2.5 μl of ×10 PCR buffer with $MgCl_2$, 0.5 μl of 10 mM dNTPs, 1 μl of dimethyl sulfoxide, and 1 μl of *Taq* polymerase. The constitutively expressed gene, *ubiquitin (UBQ*), was amplified as the internal control. The primers for *UBQ* were as follows: sense, 5′-TCGTAAGTACAATCAGGATAAGATG-3′ and antisense, 5′-CACTGAAACAAGAAAAACAAACCCT-3′. The amplification cycle consisted of pre-denaturation at 94 °C for 3 min, followed by 20 cycles of denaturation 94 °C for 30 s, primer annealing at 55 °C for 30 s, polymerization at 72 °C for 30 s, and a final extension period of 72 °C for 3 min. The primers for the *AtALMT1* ortholog were as follows: sense, 5′-CTGAAAGTAATCAGAGAATCAG-3′ and antisense, 5′-GATGGTCTCGTCTCTATAATCTT-3′ primers. PCR amplification for the *AtALMT1* ortholog was carried out as described previously (37). PCR amplification was carried out for 30 cycles consisting of denaturation at 94 °C for 30 s, primer annealing at 50 °C for 30 s, and polymerization at 72 °C for 5 min.

Statistical Analysis—Data were analyzed by Tukey's multiple comparison tests and independent samples *t* test using SPSS 18.0 software (SPSS Inc., Chicago, IL). Pearson correlation coefficients of signal co-localization were calculated using ImageJ.

RESULTS

Interspecific Variations in Nickel Tolerance and Accumulation Among Alyssum Species—Plant root growth inhibition and reduction in total plant weight are known symptoms of nickel toxicity (38). Experiments were conducted to determine the effect of varying nickel concentrations on the hyperaccumulator and non-accumulator *Alyssum* species. One-week-old plants of *A. murale* and *A. montanum* were treated with nickel at varying concentrations ranging from 0 to 1400 μM. The two species differed significantly in nickel tolerance as shown by differences in root length (Fig. 1*A*), plant weight (supplemental Fig. S1), and nickel accumulation (Fig. 1, *C* and *D*). Root growth was determined 10 days post-nickel treatment. Growth of *A. murale* roots was not affected by nickel, whereas nickel inhibited root growth of *A. montanum*. A similar trend was observed in terms of fresh weight accumulation wherein increasing con-

centrations of nickel induced toxicity in *A. montanum* compared *A. murale* plants (supplemental Fig. S1). Increase in the root length and plant weight at low concentrations of nickel at 100 and 200 μM was observed for *A. montanum*, which may be attributed to the hormesis effect (39). In addition, increasing concentrations of nickel severely reduced the growth of *A. montanum* as evident by the high percentage inhibition compared with *A. murale* (Fig. 1*B*).

For comparing nickel accumulation in both the species, roots, and shoots of plants treated with $Ni(NO_3)_2$ for different time intervals as well as untreated controls were sampled separately and oven dried at 60 °C for 2 days (Fig. 1, *C* and *D*). Nickel content was measured by ICP-AES as described under "Experimental Procedures." In *A. murale* and *A. montanum*, the nickel concentration in the root and shoot tissues increased significantly across all treatment levels compared with the untreated control. For *A. murale*, at 30 and 60 min more nickel accumulated in the roots than in leaves. However, at 5 and 10 days of post-nickel treatment, more nickel was present in the leaves compared with roots of *A. murale* plants (Fig. 1, *C* and *D*). Transfer factors were calculated as the ratio of average values of the nickel concentration in leaves to that in roots. Thus the transfer factor >1 is indicative of the ability of the plant to transfer nickel from roots to the aboveground biomass. The transfer factors for *A. murale* were 0.30, 0.57, 1.84, 2.52, and 2.80, and for *A. montanum* were 0.23, 0.37, 0.78, 0.86, and 0.89 at 30 min, 60 min, 24 h, 5 days, and 10 days, respectively. For *A. montanum* at all time intervals the transfer factor was <1, indicating that less nickel accumulated in the leaves compared with roots. Both *A. murale* and *A. montanum* did not accumulate nickel in their shoots at early time points of nickel treatment (30 and 60 min) (Fig. 1, *C* and *D*). *Alyssum* species differed markedly in their shoot nickel concentration but not in root nickel concentration at 24 h, 5 days, and 10 days treatment. *A. murale* exhibited a transfer factor >1 at 24 h, 5 days, and 10 days treatment but <1 at earlier time points (30 and 60 min). These data suggest that root to shoot transport is important and typical of nickel hyperaccumulation. Post 30 min of nickel treatment, the roots of *A. murale* accumulated more nickel compared with *A. montanum* indicating the initial root uptake is efficient in *A. murale* compared with *A. montanum.*

To compare the root physiology of *A. murale* and *A. montanum*, $Ni(NO_3)_2$ was used at the concentration of 700 μM for further experiments because it was well tolerated by both plant species. In *in vitro* growth conditions the concentration of 700 μM $Ni(NO_3)_2$ was found to be non-lethal except that it revealed a stunted growth phenotype in *A. montanum* plants compared with *A. murale*.

Differential Organelle Preference and Temporal Variability in Subcellular Compartmentalization of Nickel in Alyssum Species—Experiments were conducted to observe differences, if any, in subcellular localization and to trace translocation of nickel ions in the early events of nickel exposure in the root cells of *Alyssum* species. To directly visualize nickel ions intracellularly following root uptake, a cell permeant dye Newport Green DCF was used. Newport Green DCF is a cell permeant acetate ester that becomes fluorescent after hydrolysis. This molecule is initially uncharged, allowing it to pass through cell membranes. Once in the cell, it is hydrolyzed and becomes charged, hindering its escape from the cell and allowing it to bind charged protein-metal complexes, which then become fluorescent (40). To examine the effects of initial and prolonged nickel treatment on nickel subcellular localization in the roots of both the species, two time points, 20 and 60 min, were selected for treatment. Nickel was found to be putatively localized in root vacuoles of epithelial cells in both the species when roots were incubated with 700 μM $Ni(NO_3)_2$ for 60 min (Fig. 2, *A* and *B*). Our observation is consistent with previous reports on vacuolar sequestration of nickel in plant cells (4–8). Noticeably, more fluorescence was found to be contained in the vacuoles of *A. murale* compared with *A. montanum* root cells (Fig. 2, *A* and *B*), indicating that vacuolar nickel uptake is rapid and efficient in the roots of *A. murale* compared with *A. montanum*. In *A. montanum* a considerable amount of nickel was detected in the cell walls than in the vacuoles post 60 min of nickel treatment (Fig. 2*B*), suggesting foremost a role of cell wall binding in the chelation of nickel ions in *A. montanum*. To examine early effects of nickel treatment, roots were treated for shorter duration in both of the *Alyssum* species. No nickel was detected in the vacuoles in both *Alyssum* species when their roots were treated for $\leq$20 min. However, nickel was observed to be localized in small circular organelles ($\sim$1 μm) post 20 min of nickel administra-

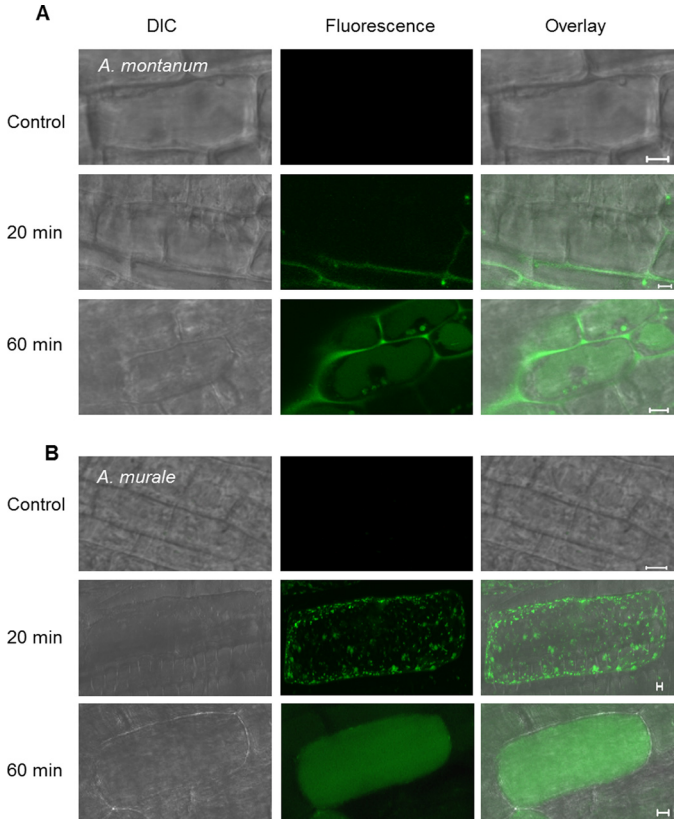

FIGURE 2. **Temporal variability in intracellular nickel sequestration in the roots of *Alyssum* species**. Confocal micrographs showing intracellular sequestration of nickel in the roots of *A. murale* (*A*) and *A. montanum* (*B*) at treatments of 20 min (*center panels*) and 1 h (*bottom panels*). Controls (*top panels*) are representative images for no nickel treatments. The roots were treated with 700 μM $Ni(NO_3)_2$ and intracellular nickel was visualized with nickel specific dye Newport Green DCF (488 nm) as shown in *left panels*. *Right panels* show differential interference contrast (*DIC*) phase images. *Scale bar* = 5 μm.

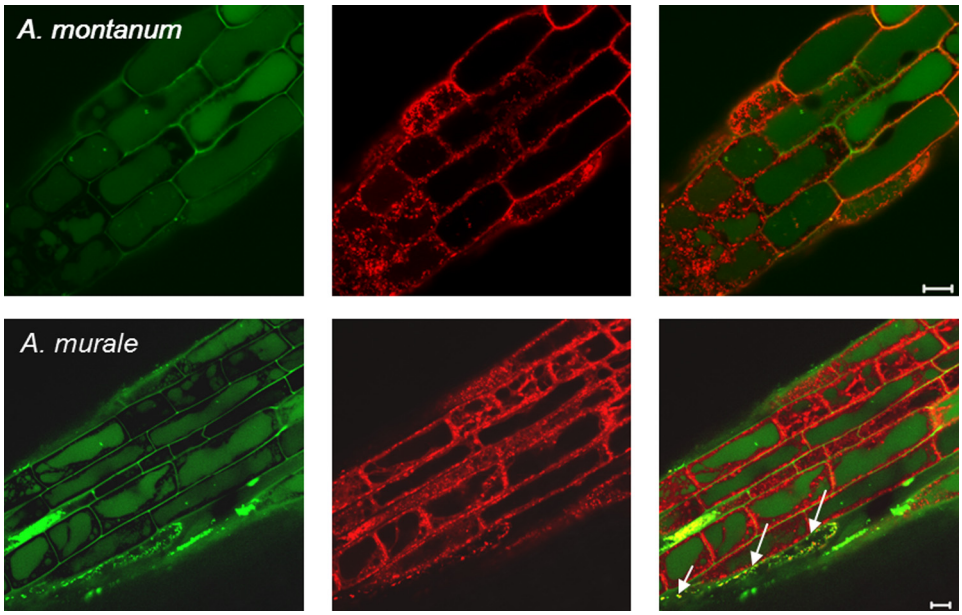

FIGURE 3. **Transient influx of nickel ions in mitochondria and sequestration to vacuoles.** Confocal micrographs showing divergence of fluorescence from nickel specific Newport Green DCF and mitochondria-specific MitoTracker Red in the roots of *A. montanum (top panel)* and *A. murale (bottom panel)*. Dual emission confocal images of Newport Green DCF and MitoTracker Red CMXRos are shown in the *left two panels*. These images are overlaid in the *two rightmost panels* to show the deviation in the patterns of the labeled organelles (*Overlay*). *Arrow bars* in *right panel* indicate dual staining of mitochondria in the roots of *A. murale*. The roots were treated with 700 μM $Ni(NO_3)_2$ for 1 h before subjecting to staining with dyes. *Scale bar* = 10 μm.

tion in *A. murale* (Fig. 2, *A* and *B*). In *A. montanum*, no such organelles were found; instead nickel ions were scarcely localized in the cell walls of root cells. Based on their shape and size, these cellular organelles at the outset were hypothesized to be vesicles, peroxisomes, mitochondria, or plastids. Because vesicles can vary in size, the possibility of them being vesicles was ruled out because these cellular organelles were consistently equal in size (41, 42). No autofluorescence (*red*) was detected from the cellular organelles indicating they were not plastids. The speculation for punctate organelles being peroxisomes and mitochondria are in agreement with their shape and size. However, peroxisomes are seldom implicated in metal ion homeostasis. Therefore, the fact that mitochondria are involved in metal ion homeostasis prompted us to conduct further experiments to determine whether they were co-localized with the nickel-labeled structures. Mitochondria in the cell can be readily labeled by MitoTracker Red CMXRos. MitoTracker Red CMXRos is a red fluorescent dye that stains mitochondria in live cells. This dye has two chloromethyl moieties that upon accumulation in the mitochondrial matrix react with thiol groups of cysteine residues and thereby becoming covalently bound to mitochondrial protein (43). To validate our observation for nickel localization in mitochondria, further experiments were conducted for qualitative and quantitative analysis of nickel localization in these cellular organelles. To determine whether these cellular organelles are mitochondria, dual labeling experiments with Newport Green DCF and MitoTracker Red CMXRos were conducted for 1 h as described under "Experimental Procedures." Vacuolar sequestration of nickel ions can be clearly seen in the roots of both the *Alyssum* species (Fig. 3). In *A. murale*, the majority of cells showed nickel sequestration in the vacuoles, whereas some of the cells were observed with mitochondria containing nickel. Interestingly, the cells exhibiting mitochondrial nickel uptake did not show nickel sequestration in the vacuoles. These observations suggest that the subcellular compartmentalization of nickel in *Alyssum* species exhibits temporal variability for the preference of the cellular organelle. In the initial steps of nickel uptake the most nickel is transiently localized in the mitochondria of the *A. murale,* whereas in the later stages it is translocated to the vacuoles. In *A. montanum* such variability is not observed at least for the above mentioned treatment durations, suggesting the importance and involvement of mitochondria in the early events of nickel uptake and its translocation in the nickel hyperaccumulator plants. The lower concentration of nickel (200 μM) tested against both *Alyssum* species showed a similar cellular pattern of nickel localization (supplemental Fig. S2). Interestingly, *A. montanum* plants treated with nickel (200 μM) showed no mitochondrial localization of nickel compared with *A. murale* at 20 and 60 min (supplemental Fig. S2). In summary, comparison of intracellular allocation of nickel ions in the roots of both *Alyssum* species revealed time-dependent variations in distribution of nickel in the cellular organelle mitochondria and vacuole. This temporal differential distribution patterns in subcellular localization indicate that subcellular sorting of nickel ions is particularly governed by the root physiology and is indicative of characteristic phenotype of nickel hyperaccumulation in plants.

Fluorescence Microscopy and Dual Labeling of Isolated Mitochondrial Fraction—To further confirm the presence of nickel in mitochondria, we set out to purify mitochondria from both *Alyssum* species, to visualize the presence of nickel using confocal microscopy and quantify the amount via ICP-AES techniques. Mitochondria isolated from the roots of untreated and nickel-treated *Alyssum* species post 20 min were visualized in a confocal microscope following dual staining with Newport

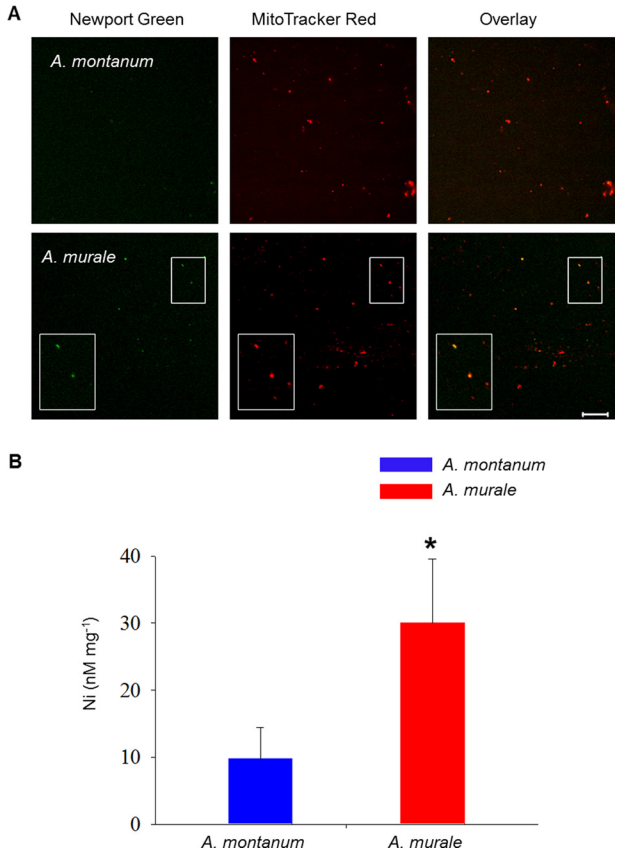

FIGURE 4. **Confirmation and quantification of mitochondrial nickel influx in purified mitochondria.** Confocal micrographs showing co-localization of fluorescence from nickel-specific Newport Green DCF and mitochondria-specific MitoTracker Red CMXRos in purified mitochondrial fractions from the roots of *A. murale* (*A*) and *A. montanum* (*B*). Dual emission confocal images of Newport Green DCF and MitoTracker Red CMXRos are shown in *left two panels*. For *A. murale*, the *inset* images show co-labeled enlarged mitochondria. These images are overlaid in the *right panel* to show the coincidence of the labeled organelles (*Overlay*). *Scale bar,* 10 μm. *C,* nickel content in root mitochondria of *Alyssum* species treated with 700 μM $Ni(NO_3)_2$ was estimated using ICP-AES. Quantitative data shows increased nickel content in mitochondria of *A. murale* compared with *A. montanum* plants. Data are expressed as nanamole of nickel mg^{-1} mitochondrial protein and represent the mean ± S.D. Data are representative of three experiments, $p < 0.05$, $n = 6$.

Green DCF and MitoTracker Red CMXRos. Mitochondria purified from the roots of treated *A. murale* plants showed the dual labeling and co-localization of both dyes, suggesting the mitochondrial-specific localization of nickel (Pearson's correlation coefficient (r_P) = 0.77 ± 0.085, $n = 12$) in *A. murale* (Fig. 4*A*). However, no co-localization was observed in the purified mitochondrial fractions of *A. montanum* (Pearson's correlation coefficient (r_P) = −0.06 ± 0.38, $n = 12$). When mitochondria isolated from *A. murale* are incubated in washing buffer (10 mM potassium phosphate, 300 mM sucrose, 1 mM EDTA, 0.1% (w/v) BSA, 5 mM glycine, pH 7.5) for >1 h, nickel diffused from the mitochondria and no nickel was detected (data not shown). Mitochondria isolated from the control plants of the both untreated *Alyssum* species (data not shown) did not exhibit staining with Newport Green DCF.

Nickel content in mitochondria extracted from roots of the control and treated *A. murale* and *A. montanum* plants was determined by ICP-AES (Fig. 4*B*) as described under "Experimental Procedures." Mean values from the mitochondrial wash buffers were subtracted to avoid the problem of carryover contamination during subcellular fractionation. An independent samples *t* test was conducted to compare nickel accumulation in isolated fractions of *A. murale* and *A. montanum.* There was a significant difference in the concentration of nickel in root mitochondria of *A. murale* (M = 30.05, S.D. = 9.5) and *A. montanum* (M = 9.8, S.D. = 4.60 plants; $t(6) = 3.82$, $p < 0.01$. The ICP-AES data clearly showed that mitochondrial fractions of *A. murale* had an ~3-fold higher concentration of nickel to non-hyperaccumulator *A. montanum* and confirms that nickel is localized in the mitochondria of nickel hyperaccumulator *A. murale* root epithelial cells during the early events of nickel uptake.

In dual labeling experiments for confocal microscopy, no nickel could be detected in the roots or isolated mitochondrial fractions of *A. montanum.* This is likely due to the low concentration of nickel ions being below detection levels in the root mitochondria of *A. montanum.* Nevertheless, the data indicate that nickel is localized transiently in root mitochondria prior to mobilization to root vacuoles. These observations led us to further investigate the role of root mitochondria in the nickel hyperaccumulation process.

Krebs Cycle Enzymatic Activities Are Modulated in Response to Nickel in Alyssum Species—The present investigations were conducted to ascertain the influence of sublethal concentrations of nickel (700 μM $Ni(NO_3)_2$) on selected enzymes of the tricarboxylic acid (TCA) cycle in *Alyssum* species. Roots were sampled at different time intervals to study a kinetic profile of the selected Krebs cycle enzymes in mitochondrial fractions of treated and untreated *Alyssum* plants. Mitochondria were isolated from the nickel-treated and -untreated roots at different time intervals. All enzymes of the Krebs cycle examined (citrate synthase and malate dehydrogenase) were found to be affected by nickel disparately in *Alyssum* species. These enzymes were particularly chosen because citric acid and malic acid have been shown to be modulated in response to nickel in different plant species (44–46). Samples heated to 100 °C for 5 min were used as blanks in all enzyme assays. All enzyme assays were carried out in triplicate. Activities of cytochrome *c* oxidase were monitored as markers to assess the purity and integrity of mitochondrial fractions. Mitochondrial preparations exhibited a negligible glucose-6-phosphate dehydrogenase activity (plastid marker enzyme) indicating the purity of mitochondrial fractions (data not shown). In addition, isolated mitochondria showed about 92–95% intactness of the outer membrane suggesting that the integrity of mitochondrial membrane was acceptable and the preparation specifically reflected the mitochondrial properties (data not shown). The enzyme activities are presented on the basis of total mitochondrial protein (Fig. 5, *A* and *C*). It should be noted that levels of enzyme activities in control *Alyssum* plant species were not similar. In *A. murale*, nickel-induced citrate synthase activity increased significantly ($p < 0.05$, $n = 3$) in 12 h, reached a plateau in 24 h, and maintained a steady level until 48 h. In *A. montanum,* citrate synthase activity decreased at 24 and 48 h in the nickel-treated plants (Fig. 5, *A–C*). Malate dehydrogenase was assayed in the forward as well as backward direction. In *A. murale*, nickel-induced malate dehydrogenase activity in the direction of oxa-

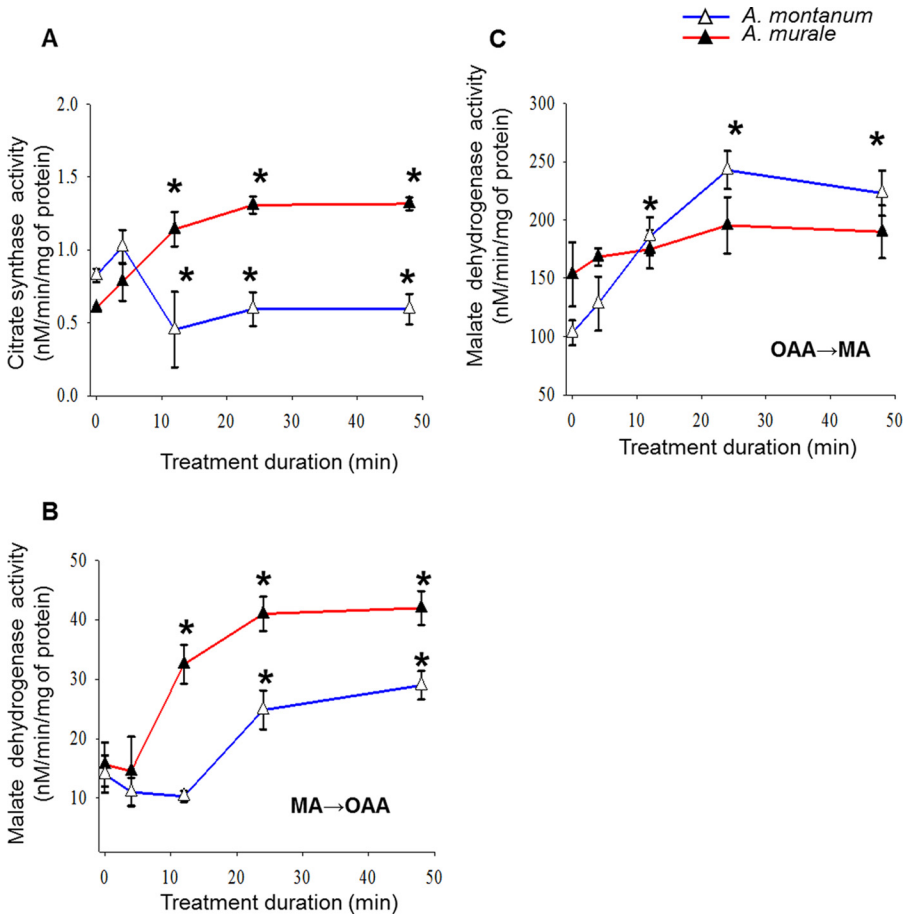

FIGURE 5. **Comparison of the effects of nickel ions on Krebs cycle in the root mitochondria of *Alyssum* species.** *A*, a kinetic investigation of citrate synthase (CS, EC 1.11.1.6) in the root mitochondrial fractions of $Ni(NO_3)_2$-treated (700 μM) hyperaccumulator *A. murale* and comparison with *A. montanum*. *B,* a kinetic investigation of *malate dehydrogenase* activity in the direction of NADH oxidation (MDH, EC 1.1.1.37) in the root mitochondrial fractions of $Ni(NO_3)_2$-treated (700 μM) hyperaccumulator *A. murale* and comparison with *A. montanum*. *C,* a kinetic investigation of *malate dehydrogenase* activity in the direction of malate oxidation (EC 1.1.1.37) in the root mitochondrial fractions of $Ni(NO_3)_2$-treated (700 μM) hyperaccumulator *A. murale* and comparison with *A. montanum*. Total enzymatic activities are expressed as nanamolar/min/mg of mitochondrial protein. Results are the average of three independent determinations ± S.D. *, indicates significant difference from control, $p < 0.05$).

loacetate formation was significantly increased ($p < 0.05$, $n = 3$) in 12, 24, and 48 h (Fig. 5, *A–C*). In *A. montanum*, nickel-induced malate dehydrogenase activity in the direction of oxaloacetate formation increased at 24- and 48-h treatment durations (Fig. 5, *A–C*). In *A. murale*, nickel-induced malate dehydrogenase activity in the direction of malate formation was found to be significantly higher ($p < 0.05$, $n = 3$) in 12 to 48 h (Fig. 5, *A–C*). In *A. montanum,* changes in nickel-induced malate dehydrogenase activity in the direction of malate formation were insignificant compared with control. It is interesting to note that in *A. murale*, malate dehydrogenase activity in the forward direction (in the direction of NADH oxidation) was highly favored compared with the backward direction (in the direction of NAD^+ reduction). Overall there was an increase in the malate dehydrogenase activity in both directions in mitochondria of *A. murale* but not *A. montanum*.

Previous studies have shown that overexpression of malate dehydrogenase increases secretion of organic acids including malic acid and confers enhanced tolerance to aluminum in transgenic *Medicago sativum* (47). In addition, aluminum-induced malate transporter (*AtALMT1*) encodes malate transporter that is associated with malate efflux and aluminum tolerance (37, 48). Because our results showed that nickel uptake elicits malic acid biosynthesis in roots, we next examined whether *AtALMT1*, a plasma membrane-located malic acid transporter, is involved in nickel hyperaccumulation. To that end, we checked expressions levels of the *AtALMT1* ortholog in response to nickel in the roots of *A. murale* and *A. montanum*. Nickel does not induce expression of the *AtALMT1* ortholog in the roots of *A. murale* or *A. montanum* (supplemental Fig. S3), indicating specificity of the *AtALMT1* ortholog for aluminum over divalent nickel ions.

Intracellular Malic Acid Reduces Generation of ROS in Treated Roots—To elucidate the role of intracellular malic acid in detoxification of nickel ions; ROS generation was estimated in nickel-treated roots preincubated with malic acid. Nickel ions form complexes with malate in several hyperaccumulators including *Alyssum bertolonii* (49), *Psychotria douarrei, Phyllanthus serpentinus* (50), *Sebertia acuminate* (51), *Dichapetalum gelonioides* (52), and *A. murale* (46, 53). To investigate the effect of intracellular malic acid on ROS, *Alyssum* roots were either preincubated with malic acid (50 μM) for 1 h or left untreated (control). At the end of the preincubation roots were washed with 3% MS medium to remove excess malic acid. Con-

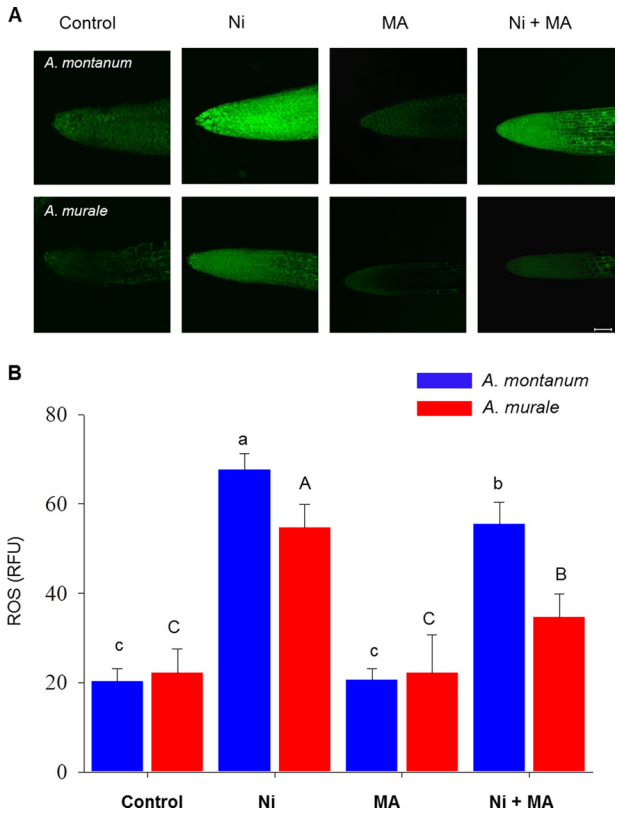

FIGURE 6. **Malic acid reduces generation of ROS in nickel-treated *Alyssum* roots.** *A*, intracellular ROS production was monitored with H_2DCFDA in control and treated roots and compared with ROS generated in the roots preincubated with malic acid (*MA*). Images were acquired using identical parameters on a Zeiss Meta 510 confocal microscope using a ×10 objective; post-processing and analysis was done with ImageJ. *Scale bar* = 50 μm. *B*, quantization of fluorescence from images by using ImageJ. *RFU*, relative fluorescence unit. Significant differences among the treatments at $p < 0.05$ were determined by one-way analysis of variance followed by Tukey-Kramer test ($\alpha = 0.5$) and are indicated by *different letters*.

trol roots were also washed similarly to avoid experimental variation. Both malic acid preincubated and control roots of *A. murale* and *A. montanum* were treated with nickel or no nickel. The nickel-induced ROS production was monitored by imaging the ROS-sensitive fluorescent dye, H_2DCFDA, which revealed that nickel (80 μM) induces a rapid increase in ROS in both *Alyssum* species post 60 min of treatment (Fig. 6*A*). The DCF-based imaging *in vivo* indicated that nickel elicits a burst of ROS in both *Alyssum* species, predominantly in the root tip and the central elongation regions (Fig. 6*A*). Having shown that nickel induces ROS response in both the hyperaccumulator and non-hyperaccumulator species, we next attempted to block intracellular ROS production using malic acid to characterize its role in nickel-induced toxicity. Malic acid in combination with nickel blocked the ROS generation seen in response to nickel (Fig. 6*B*) in both species. Furthermore, *A. murale* roots co-treated with nickel and malic acid exhibited less ROS generation compared with similarly treated roots of *A. montanum* (Fig. 6*B*), suggesting the direct involvement of malic acid in diminishing nickel-induced ROS in the hyperaccumulator plants.

DISCUSSION

The purpose of the present study is to investigate the potential role of root mitochondria in maintaining homeostasis in the early steps of nickel uptake in hyperaccumulator plants. To achieve this objective, a comparative approach was employed to investigate function of mitochondria in the roots of similarly treated non-accumulator and hyperaccumulator plants. Typically, Genus and family taxonomic groupings are expected to show similar tolerance responses among species. Interestingly, the two plant species belonging to the family *Cruciferae* and Genus *Alyssum* differ strikingly in nickel tolerance. *A. murale* is highly tolerant of nickel compared with *A. montanum* (2, 54). In addition to exhibiting tolerance to high concentrations of nickel, *A. murale* has a remarkable ability to accumulate and store nickel up to 1–3% of its dry biomass (54). This unusual physiological adaptation of *A. murale* makes its classification as a nickel hyperaccumulator.

Instead of the leaf system; which is a common focus in most of the studies, the root system of the plants was chosen because roots are the first line of contact to nickel in soil. Root tissue must mount a specific and coordinated response when it first comes in contact with heavy metal nickel ions. This response must vary in both hyperaccumulators and non-accumulator plant roots. Response of hyperaccumulators and non-accumulators to nickel in the early steps of treatment is not categorized. In the roots of the hyperaccumulator *A. murale*, vacuolar compartmentalization of nickel was clearly observed by confocal microscopy 1 h post-nickel treatment. Similarly, non-accumulator *A. montanum* also stored nickel in the vacuoles, however, it exhibited less efficient storage of nickel in the vacuoles (Fig. 2, *A* and *B*). Thus, vacuolar sequestration of nickel occurs not only in the nickel hyperaccumulator, *A. murale,* but also in non-accumulator plants such as *A. montanum*. Therefore, the root cell vacuolar sequestration of nickel is not a definite criterion that distinguishes physiologically between hyperaccumulator and non-accumulator plants. To reach the vacuoles, nickel should be concentrated in the cytosol and should be escorted to the vacuoles in a detoxified form. Nickel has been proposed to be escorted to the vacuoles in the form of metal-organic acid complexes (55). In its travel from the plasma membrane to cytosolic vacuoles nickel ions and/or nickel-organic acid complexes are likely to come in contact with other cellular organelles. We hypothesized that the initial physiological and biochemical differences of plants in nickel uptake in roots should differentiate between the hyperaccumulators and non-accumulators. The initial response of the hyperaccumulators to nickel in the root cells following uptake of nickel is crucial for hyperaccumulation. It is anticipated that to avoid the toxic effects the plant roots of hyperaccumulators may adapt to high a concentration of nickel ions in the early steps of nickel uptake itself. To our knowledge, there no studies investigating the early translocation of nickel through roots and its accumulation in the root cells of hyperaccumulators species.

We observed differences in subcellular localization of nickel in the roots of the *Alyssum* species in early (20 min) and prolonged (≥1 h) nickel treatments (Fig. 2, *A* and *B*). The argument that the variation in time-dependent spatial localization is due to toxic conditions is ruled out because *A. murale* can withstand much higher concentrations of nickel (>1 mM $Ni(NO_3)_2$) than used in the experimental conditions (700 μM, $Ni(NO_3)_2$). Our study demonstrates that in the initial steps of nickel treat-

ment, rapid and transient influx of nickel takes place in the root mitochondria of hyperaccumulator *A. murale*. Previously, in mitochondria metal ions, such as Mg^{2+} transport, processes have been shown to play an important role in cellular homeostasis and in the regulation of cell and mitochondrial functions in other systems (56). Interestingly, mitochondrial Mg^{2+} pools are mobilized to adjust cytoplasmic pools and overexpression of *Mrs2p* increased influx rates in mitochondria (57). Brooks *et al.* (62), demonstrated the presence of nickel in mitochondria of *Alyssum serpyllifolium* leaves, showing ~2% of total nickel concentrations were allocated to the mitochondria in nickel hyperaccumulators. Interestingly, a putative mitochondrial processing peptidase (NP_186858) was the only protein that increased in abundance after both short (24 h) and long term (28 days) exposure to nickel in *Alyssum lesbiacum* (21) asserting the role of mitochondria in early adaptation to nickel ions in hyperaccumulators. Mitochondrial processing peptidase is a metalloendopeptidase that plays an essential role in mitochondrial protein import. It cleaves the N-terminal signal sequences of nuclear-encoded proteins targeted for transport from the cytosol to the mitochondria.

Knowledge of the effects of nickel on subcellular organelle functions should aid in understanding the mechanisms of nickel hyperaccumulation. Because mitochondria are the important targets in heavy metal toxicity in plants and animals, hyperaccumulators should have a mechanism to avoid the toxic effects of metals in mitochondria. Transition metal ions are indispensable for many aspects of the mitochondrial functioning. Although association of metals with mitochondria has long been explored, the role of mitochondria in the metal hyperaccumulation process is not known. Therefore, in this study emphasis was placed on the study of mitochondrial function in response to nickel in the *Alyssum* species. One of the most important functions of mitochondria in all known organisms is synthesis of chemical energy via Krebs cycle. As chemical energy is synthesized via the Krebs cycle in plants, organic acids are produced and their metabolic levels are constantly regulated. With respect to metabolic processes in mitochondria the role of organic acids as detoxifying agents in the matrix and outside of these organelles are of particular interest.

At least two organic acids of the Krebs cycle, malic acid and citric acid, are known to play an important role in the hyperaccumulation process by forming of complexes with nickel. Brooks *et al.* (62), suggested the possibility of production of malic acid as the tolerance mechanism in the nickel hyperaccumulator, *A. serpyllifolium.* A few studies have reported basal high levels of organic acids in the nickel hyperaccumulators (58–60) in different plant species. There is sufficient evidence that organic acid-metal complexes may play a role in metal hyperaccumulation process (44, 53, 59). Complexation of metals with organic acids is achieved to reduce free metal ionic activity. Detoxification of nickel ions by organic acid(s) is important for nickel uptake, translocation, sequestration, and storage. It has been suggested that nickel is stored in the vacuoles by binding to organic acids. In vacuoles, malic acid and citric acid chelate nickel for its storage in the detoxified form (8, 61, 62). Involvement of two organic acids of the Krebs cycle, citric and malic acid, in the hyperaccumulation process may not be merely coincidental. Enzymes are one of the main targets of heavy metal ions and prolonged exposure of roots to heavy metals results in marked decreases in root enzyme activity leading to speculations that different enzymes in the Krebs cycle may have role in hyperaccumulation (62). Considering that Krebs cycle metabolism impairment is probably involved in the nickel-induced toxicity, we speculated that an increase in metabolism by nickel in *A. murale* could be an important mechanism of counteracting toxicity. There are several enzymes known that contain nickel as an active site or cofactor (63, 64). However, none of these enzymes have a role in the Krebs cycle. Analysis of the Krebs cycle enzymes indicated that malate dehydrogenase and citrate synthase enzymatic activities were modulated differently in the hyperaccumulator and non-accumulator *Alyssum* species (Fig. 5, *A–C*) indicating the Krebs cycle in root cells respond separately to nickel exposure in these two plant species.

Mitochondria are key cellular organelles in plant cell redox homeostasis and signaling (65). It is well established that mitochondria are important regulators of apoptosis and undergo major changes during apoptotic cell death. Changes in the mitochondrial membrane potential due to enhanced generation of ROS and/or the depletion of reduced glutathione (GSH) induce opening of the mitochondrial permeability transition pore and the release of cytochrome *c* from the mitochondria to the cytosol. The release of cytochrome *c* from mitochondria is a key factor in an early event in programmed cell death in plant cells (66, 67). Interestingly, elevated GSH concentrations, driven by constitutively elevated serine acetyltransferase activity, are involved in conferring tolerance to nickel-induced oxidative stress in nickel hyperaccumulator *Thlaspi* species (68). Investigation of effects of malic acid on ROS revealed that malic acid reduces the effect of nickel-induced ROS in the roots of *A. murale* compared with *A. montanum*. One possible explanation for this observation could be formation of intracellular coordination complex of malic acid with nickel ions (46, 49–53), which reduces free ion activity and thereby modulates ROS. In a previous study, malic acid reduced ROS in the early steps of apoptosis induction in protoplasts (19).

We propose that transient nickel trafficking is imperative for regulation of Krebs cycle and ROS production (Fig. 7) in the root mitochondria of nickel hyperaccumulators. Specifically, nickel regulates mitochondrial Krebs cycle enzymes such as, malate dehydrogenase and citrate synthase in the mitochondria of the roots of these plants. Such regulation is absent in the roots of non-accumulator *A. montanum* rendering them susceptible to nickel. This regulation of Krebs cycle enzymes may be initiated by either direct or indirect interaction of nickel with Krebs cycle components. For direct interaction of Krebs cycle components with nickel, it should be localized in mitochondria. Nickel may regulate the Krebs cycle in hyperaccumulators irrespective of its localization in mitochondria and its direct interaction with Krebs cycle components. However, finding that nickel is localized in mitochondria supports the notion that nickel is directly involved in Krebs cycle regulation in the nickel hyperaccumulator species. Further studies, such as identification of a nickel-stimulated ion channel protein in mitochondria, are required to validate the present findings as well as to

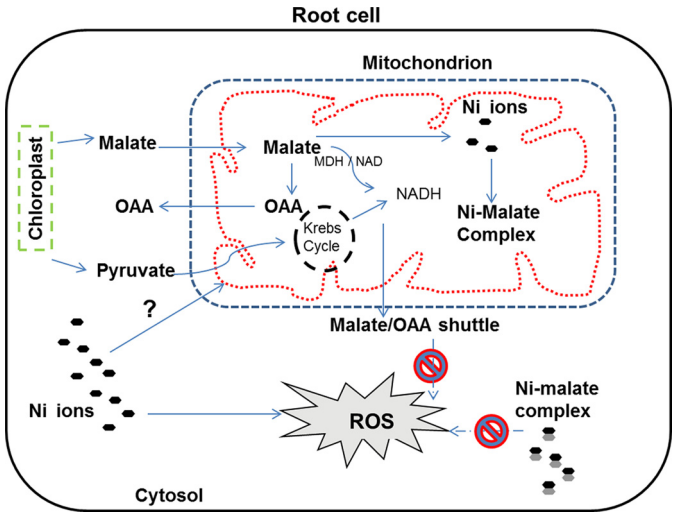

FIGURE 7. **Schematic of the proposed model for the role of mitochondrial nickel influx in tolerance and hyperaccumulation.** The scheme denotes the transient nickel influx in root mitochondria of nickel hyperaccumulator plants, which are proposed to participate in modulation of organic acid and ROS production. The root epithelial cells of nickel hyperaccumulator play a significant role in nickel mobilization and storage *in planta*. Krebs cycle intermediates, specifically malic acid production, are up-regulated resulting in efflux of malic acid from mitochondria via malic acid shuttle. Intracellular malic acid may bind to nickel ions to form complexes and/or by an unknown mechanism(s) suppresses nickel-induced ROS and prevents apoptosis of the root cells.

better elucidate the relationship between nickel exposure and mitochondria in nickel hyperaccumulators. Elucidation of the mechanism involved in the management of mitochondrial toxicity in hyperaccumulator plants may provide further insight into engineering toxic metal evasion in crop plants.

REFERENCES

1. Chaney, R. L., Angle, J. S., Broadhurst, C. L., Peters, C. A., Tappero, R. V., and Sparks, D. L. (2007) Improved understanding of hyperaccumulation yields commercial phytoextraction and phytomining technologies. *J. Environ. Qual.* **36,** 1429–1443
2. Baker, A. J., and Brooks, R. R. (1989) Terrestrial higher plants which hyperaccumulate metallic elements. A review of their distribution, ecology, and phytochemistry. *Biorecovery* **1,** 81–126
3. Baker, A. J. M., S. P. McGrath, R. D. Reeves, and Smith., J. A. C. (2000) in *Phytoremediation of Contaminated Soil and Water* (Terry, N., and Banuelos, G., eds) pp. 85–107, Lewis Publishing, Boca Raton, FL
4. Asemaneh, T., Ghaderian, S. M., Crawford, S. A., Marshall, A. T., and Baker, A. J. (2006) Cellular and subcellular compartmentation of nickel in the Eurasian serpentine plants *Alyssum bracteatum*, *Alyssum murale* (Brassicaceae) and *Cleome heratensis* (Capparaceae). *Planta* **225,** 193–202
5. Saito, A., Saito, M., Ichikawa, Y., Yoshiba, M., Tadano, T., Miwa, E., and Higuchi, K. (2010) Difference in the distribution and speciation of cellular nickel between nickel-tolerant and non-tolerant *Nicotiana tabacum* L. cv. BY-2 cells. *Plant Cell Environ.* **33,** 174–187
6. Küpper, H., Lombi, E., Zhao, F. J., Wieshammer, G., and McGrath, S. P. (2001) Cellular compartmentation of nickel in the hyperaccumulators *Alyssum lesbiacum*, *Alyssum bertolonii* and *Thlaspi goesingense*. *J. Exp. Bot.* **52,** 2291–2300
7. Bidwell, S. D., Crawford, S. A., Woodrow, I. E., Sommer-Knudsen, J., and Marshall, A. T. (2004) Subcellular localization of Ni in the hyperaccumulator, *Hybanthus floribundus* (Lindley F. Murell. *Plant Cell Environ.* **27,** 705–716
8. Krämer, U., Pickering, I. J., Prince, R. C., Raskin, I., and Salt, D. E. (2000) Subcellular localization and speciation of nickel in hyperaccumulator and non-accumulator *Thlaspi* species. *Plant Physiol.* **122,** 1343–1353
9. Kramer, U., Cotter-Howells, J. D., Charnock, J. M., Baker, A. J., and Smith, J. A. (1996) Free hisindine as a metal chelator in plants that accumulate nickel. *Nature* **379,** 635–638
10. Kerkeb, L., and Krämer, U. (2003) The role of free histidine in xylem loading of nickel in *Alyssum lesbiacum* and *Brassica juncea*. *Plant Physiol.* **131,** 716–724
11. Douchkov, D., Gryczka, C., Stephan, U. W., Hell, R., and Bäumlein, H. (2005) Ectopic expression of nicotinamine synthase genes results in improved iron accumulation and increased nickel tolerance in transgenic tobacco. *Plant Cell Environ.* **28,** 365–374
12. Riesen, O., and Feller, U. (2005) Redistribution of nickel, cobalt, manganese, zinc and cadmium via the phloem in young and maturing wheat. *J. Plant Nutr.* **28,** 421–430
13. Tappero, R., Peltier, E., Gräfe, M., Heidel, K., Ginder-Vogel, M., Livi, K. J., Rivers, M. L., Marcus, M. A., Chaney, R. L., and Sparks, D. L. (2007) Hyperaccumulator *Alyssum murale* relies on a different metal storage mechanism for cobalt than for nickel. *New Phytol.* **175,** 641–654
14. de la Fuente, V., Rodriguez, N., Diez-Garretas, B., Rufo, L., Asensi, A., and Amils, R. (2007) Nickel distribution in the hyperaccumulator *Alyssum serpyllifolium* Desf. spp. from the Iberian peninsula. *Plant Biosystems* **141,** 170–180
15. Berazain, R., de la Fuente, V., Rufo, L., Rodriguez, N., Amils, R., Diez-Garretas, B., Sanchez-Mata, D., and Asensi, A. (2007) Nickel localization in tissues of different hyperaccumulator species of Euphorbiaceae from ultramafic areas of Cuba. *Plant Soil* **293,** 99–106
16. Mesjasz-Przybylowicz, J., Barnabas, A., and Przybylowicz, W. (2007) Comparision of cytology and distribution of nickel in roots of Ni hyperaccumulating and non-hyperaccumulating genotypes of *Senecio coronatus*. *Plant Soil* **293,** 61–78
17. Smart, K. E., Kilburn, M. R., Salter, C. J., Smith, J. A. C., and Grovenor, C. R. (2007) NanoSIMS and EPMA analysis of nickel localization in leaves of the hyperaccumulator plant *Alyssum lesbiacum*. *Int. J. Mass Spectrom.* **260,** 107–114
18. Bhatia, N. P., Walsh, K. B., Orlic, I., Siegele, R., Ashwath, N., and Baker, A. J. (2004) Studies on spatial distribution of nickel in leaves and stems of the metal hyperaccumulator *Stackhousia tryonii* using nuclear microprobe (microPIXE) and EDXS techniques. *Funct. Plant Biol.* **31,** 1061–1074
19. Weir, I. E., Pham, N.-A., and Hedley, D. W. (2003) Oxidative stress is generated via the mitochondrial respiratory chain during plant cell apoptosis. *Cytometry* **54A,** 109–117
20. Gomes-Junior, R. A., Moldes, C. A., Delite, F. S., Gratão, P. L., Mazzafera, P., Lea, P. J., and Azevedo, R. A. (2006) Nickel elicits a fast antioxidant response in *Coffea arabica* cells. *Plant Physiol. Biochem.* **44,** 420–429
21. Ingle, R. A., Smith, J. A., and Sweetlove, L. J. (2005) Responses to nickel in the proteome of the hyperaccumulator plant *Alyssum lesbiacum*. *Biometals* **18,** 627–641
22. Pompeu, G. B., Gratao, P. L., Vitorello, V. A., and Azevedo, R. A. (2008) Antioxidant isoenzyme responses to nickel-induced stress in tobacco cell suspension culture. *Sci. Agric.* **65,** 548–552
23. Pierrel, F., Cobine, P. A., and Winge, D. R. (2007) Metal ion availability in mitochondria. *Biometals* **20,** 675–682
24. Foreman, J., Demidchik, V., Bothwell, J. H., Mylona, P., Miedema, H., Torres, M. A., Linstead, P., Costa, S., Brownlee, C., Jones, J. D., Davies, J. M., and Dolan, L. (2003) Reactive oxygen species produced by NADPH oxidase regulate plant cell growth. *Nature* **422,** 442–446
25. Joo, J. H., Bae, Y. S., and Lee, J. S. (2001) Role of auxin-induced reactive oxygen species in root gravitropism. *Plant Physiol.* **126,** 1055–1060
26. Randhawa, V. K., Zhou, F., Jin, X., Nalewajko, C., and Kushner, D. J. (2001) Role of oxidative stress and thiol antioxidant enzymes in nickel toxicity and resistance in strains of the green alga *Scenedesmus acutus f. alternans*. *Can. J. Microbiol.* **47,** 987–993
27. Kumar, P., Tewari, R. K., and Sharma, P. N. (2007) Excess nickel-induced changes in antioxidative processes in maize leaves. *J. Plant Nutr. Soil Sci.* **170,** 796–802
28. Hao, F. S., Wang, X. C., and Chen, J. (2006) Involvement of plasma-membrane NADPH oxidase in nickel-induced oxidative stress in roots of wheat seedlings. *Plant Sci.* **170,** 151–158

29. Neuburger, M., Journet, E. P., Bligny, R., Carde, J. P., and Douce, R. (1982) Purification of plant mitochondria by isopycnic centrifugation in density gradients of Percoll. *Arch Biochem. Biophys.* **217,** 312–323
30. Bradford, M. M. (1976) A rapid and sensitive method for the quantitation of microgram quantities of protein utilizing the principle of protein-dye binding. *Anal. Biochem.* **72,** 248–254
31. Ian, M. M., and John, M. P. (1982) Direct evidence for the presence of a rotenone-resistant NADH dehydrogenase on the inner surface of the inner membrane of plant mitochondria. *Physiol. Plant.* **54,** 267–274
32. Stephanie, C. A., Natalia, V. B., Abir, U. I., and Ian, M. M. (1998) The internal rotenone-insensitive NADPH dehydrogenase contributes to malate oxidation by potato tuber and pea leaf mitochondria. *Physiol. Plant.* **104,** 329–336
33. Veeger, C., Der Vartaniand, V., and Zeylemaker, W. P. (1969) Succinate dehydrogenase. *Methods Enzymol.* **13,** 81–90
34. Morgunov, I., and Srere, P. A. (1998) Interaction between citrate synthase and malate dehydrogenase. Substrate channeling of oxaloacetate. *J. Biol. Chem.* **273,** 29540–29544
35. Ochoa, S. (1955) *Methods in Enzymology,* Vol. 1, Academic Press, Inc., New York
36. Murphey, W. H., and Kitto, G. B. (1969) Malate dehydrogenase from *Escherichia coli*. *Methods Enzymol.* **13,** 145–150
37. Kobayashi, Y., Hoekenga, O. A., Itoh, H., Nakashima, M., Saito, S., Shaff, J. E., Maron, L. G., Piñeros, M. A., Kochian, L. V., and Koyama, H. (2007) Characterization of AtALMT1 expression in aluminum-inducible malate release and its role for rhizotoxic stress tolerance in *Arabidopsis*. *Plant Physiol.* **145,** 843–852
38. Chen, C., Huang, D., and Liu, J. (2009) Functions and toxicity of nickel in plants. Recent advances and future prospects. *CLEAN Soil Air Water* **37,** 304–313
39. Kaiser, J. (2003) Hormesis. Sipping from a poisoned chalice. *Science* **302,** 376–369
40. Zhao, J., Bertoglio, B. A., Devinney, M. J., Jr., Dineley, K. E., and Kay, A. R. (2009) The interaction of biological and noxious transition metals with the zinc probes FluoZin-3 and Newport Green. *Anal. Biochem.* **384,** 34–41
41. Rafelski, S. M., and Marshall, W. F. (2008) Building the cell. Design principles of cellular architecture. *Nat. Rev. Mol. Cell Biol.* **9,** 593–602
42. Xu, T., and Bajjalieh, S. M. (2001) SV2 modulates the size of the readily releasable pool of secretory vesicles. *Nat. Cell Biol.* **3,** 691–698
43. Scorrano, L., Petronilli, V., Colonna, R., Di Lisa, F., and Bernardi, P. (1999) Chloromethyltetramethylrosamine (Mitotracker Orange) induces the mitochondrial permeability transition and inhibits respiratory complex I. Implications for the mechanism of cytochrome *c* release. *J. Biol. Chem.* **274,** 24657–24663
44. Lee, J., Reeves, R. D., Brooks, R. R., and Jaffré, T. (1977) Isolation and identification of a citrato-complex of nickel from nickel accumulating plants. *Phytochemistry* **16,** 1503–1505
45. Sagner, S., Kneer, R., Wanner, G., Cosson, J.-P., Deus-Neumann, B., and Zenk, M. H. (1998) Hyperaccumulation, complexation and distribution of nickel in *Sebertia acuminata*. *Phytochemistry* **47,** 339–347
46. Montargès-Pelletier, E., Chardot, V., Echevarria, G., Michot, L. J., Bauer, A., and Morel, J.-L. (2008) Identification of nickel chelators in three hyperaccumulating plants. An x-ray spectroscopic study. *Phytochemistry* **69,** 1695–1709
47. Tesfaye, M., Temple, S. J., Allan, D. L., Vance, C. P., and Samac, D. A. (2001) Overexpression of malate dehydrogenase in transgenic alfalfa enhances organic acid synthesis and confers tolerance to aluminum. *Plant Physiol.* **127,** 1836–1844
48. Delhaize, E., Ryan, P. R., Hebb, D. M., Yamamoto, Y., Sasaki, T., and Matsumoto, H. (2004) Engineering high-level aluminum tolerance in barley with the *ALMT1* gene. *Proc. Natl. Acad. Sci. U.S.A.* **101,** 15249–15254
49. Pelosi, P., Fiorentini, R., and Galoppini, C. (1976) On the nature of nickel compounds in *Alyssum bertolonii. AgricBiol. Chein.* **40,** 1641
50. Kersten, W. J., Brooks, R. R., Reeves, R. D., and Jaffré, A. (1980) Nature of nickel complexes in *Psychotria douarrei* and other nickel-accumulating plants. *Phytochemistry* **19,** 1963–1965
51. Callahan, D. L., Roessner, U., Dumontet, V., Perrier, N., Wedd, A. G., O'Hair, R. A., Baker, A. J., and Kolev, S. D. (2008) LC-MS and GC-MS metabolite profiling of nickel(II) complexes in the latex of the nickel-hyperaccumulating tree *Sebertia acuminata* and identification of methylated aldaric acid as a new nickel(II) ligand. *Phytochemistry* **69,** 240–251
52. Homer, F. A., Reeves, R. D., Brooks, R. R., and Baker, A. J. M. (1991) Characterization of the nickel-rich extract from the nickel hyperaccumulator *Dichapetalum gelonioides*. *Phytochemistry* **30,** 2141–2145
53. McNear, D. H., Jr., Chaney, R. L., and Sparks, D. L. (2010) The hyperaccumulator *Alyssum murale* uses complexation with nitrogen and oxygen donor ligands for nickel transport and storage. *Phytochemistry* **71,** 188–200
54. Brooks, R. R., Morrison, R. S., Reeves, R. D., Dudley, T. R., and Akman, Y. (1979) Hyperaccumulation of nickel by *Alyssum linnaeus* (Crucifarae). *Proc. R. Soc. Lond. Ser. B Biol. Sci.* **203,** 387–403
55. Krämer, U., Talke, I. N., and Hanikenne, M. (2007) Transition metal transport. *FEBS Lett.* **581,** 2263–2272
56. Romani, A. M., and Scarpa, A. (2000) Regulation of cellular magnesium. *Front. Biosci.* **5,** D720-D734
57. Kolisek, M., Zsurka, G., Samaj, J., Weghuber, J., Schweyen, R. J., and Schweigel, M. (2003) Mrs2p is an essential component of the major electrophoretic Mg^{2+} influx system in mitochondria. *EMBO J.* **22,** 1235–1244
58. Boyd, R., and Martens, S. (1998) Nickel hyperaccumulation by *Thlaspi montanum* var. *montanum* (*Brassicaceae*). A constitutive trait. *Am. J. Bot.* **85,** 259–265
59. Lee, J., Reeves, R. D., Brooks, R. R., and Jaffré, T. (1978) The relation between nickel and citric acid in some nickel-accumulating plants. *Phytochemistry* **17,** 1033–1035
60. Boominathan, R., and Doran, P. M. (2003) Organic acid complexation, heavy metal distribution and the effect of ATPase inhibition in hairy roots of hyperaccumulator plant species. *J. Biotechnol.* **101,** 131–146
61. Perrier, N., Colin, F., Jaffré, T., Ambrosi, J.-P., Rose, J., and Bottero, J.-Y. (2004) Nickel speciation in *Sebertia acuminata*, a plant growing on a lateritic soil of New Caledonia. *C. R. Geosciences* **336,** 567–577
62. Brooks, R., Shaw, S., and Marfil, A. A. (1981) The chemical form and physiological function of nickel in some Iberian *Alyssum* species. *Physiol. Plant.* **51,** 167–170
63. Ermler, U., Grabarse, W., Shima, S., Goubeaud, M., and Thauer, R. K. (1998) Active sites of transition-metal enzymes with a focus on nickel. *Curr. Opin. Struct. Biol.* **8,** 749–758
64. Küpper, H., and Kroneck, P. M. H. (2007) in *Metal Ions in Life Sciences* (Sigel, A., Sigel, H., and Sigel, R. K. O., eds) pp. 31–62, John Wiley and Sons, Chichester, UK
65. Noctor, G., De Paepe, R., and Foyer, C. H. (2007) Mitochondrial redox biology and homeostasis in plants. *Trends Plant Sci.* **12,** 125–134
66. Balk, J., Leaver, C. J., and McCabe, P. F. (1999) Translocation of cytochrome c from the mitochondria to the cytosol occurs during heat-induced programmed cell death in cucumber plants. *FEBS Lett.* **463,** 151–154
67. Balk, J., and Leaver, C. J. (2001) The PET1-CMS mitochondrial mutation in sunflower is associated with premature programmed cell death and cytochrome *c* release. *Plant Cell Online* **13,** 1803–1818
68. Freeman, J. L., Persans, M. W., Nieman, K., Albrecht, C., Peer, W., Pickering, I. J., and Salt, D. E. (2004) Increased glutathione biosynthesis plays a role in nickel tolerance in thlaspi nickel hyperaccumulators. *Plant Cell* **16,** 2176–2191